Modeling Wet-Gas Annular/Dispersed Flow Through a Venturi

M. van Werven and H. R. E. van Maanen
Shell International Exploration and Production, Technical Applications and Research,
2280 AB Rijswijk, The Netherlands

G. Ooms
J. M. Burgers Centre, Laboratory for Aero and Hydrodynamics, Delft University of Technology,
2628 CJ Delft, The Netherlands

B. J. Azzopardi
School of Chemical, Environmental and Mining Engineering, University of Nottingham,
Nottingham NG7 2RD, U.K.

A theoretical model for gas–liquid annular/dispersed flow through a venturi meter is reported. It is based on an earlier model developed for venturi scrubbers. Changes implemented are based on new research and on the different physics between the two cases. The predictions of the model have been tested using information from recent experiments on venturi meters employed for measuring wet-gas flows with a liquid volume fraction up to 10%. The model gives good predictions with appropriate values of a small set of input variables.

Introduction

The convergent/divergent geometry commonly named after Giovanni Baptista Venturi has been widely used as a single-phase flow-measurement device in pipelines, achieving a high accuracy with a simple and robust design. The use of a venturi meter to measure the flow rate of a liquid–solid flow (a flow of a liquid with particles) in a pipeline was first researched nearly 40 years ago (Brook, 1962). Graf (1967) proposed that the flow rates of both phases could be determined from the pressure drop to the throat and the overall pressure loss across the venturi. Further work on this has been produced by Hirata et al. (1991, 1995).

The use of a venturi as meter for a gas–liquid flow (a flow of a gas with liquid) in a pipeline has also been studied for a long time (Thompson et al., 1966; Harris, 1967). It is still a subject of research (Machado, 1997; Pinhero da Silva Filho, 2000; Hall et al., 2000). Recent work has employed the venturi, together with another independent measurement device, in order to determine the gas and liquid flow rates. However, to the best of our knowledge, measurement of the gas and liquid flow rates in a pipeline with a venturi only is still not generally possible.

Our plan is to develop a method to make such a measurement possible for so-called wet-gas flows, for which the mass flow rate of the liquid is not larger than that of the gas. Because the liquid density is considerably higher than the gas density, the liquid volume fraction is not more than a few percent. Moreover the gas velocity is assumed to be high enough for the flow pattern in the pipeline and in the venturi to be annular/dispersed. The idea is to measure the pressure drop up to the venturi throat and up to the end of the venturi, and using a theoretical model in inversion, to derive from these two measurements, the mass flow rates of the gas and the liquid.

For this it is essential to have an accurate theoretical model for annular/dispersed flow of a wet gas through a venturi. To that purpose an existing theoretical model published in the open literature has been extended. This theoretical model was originally developed for describing the annular/dispersed gas–liquid flow in a venturi scrubber, in order to predict the pressure drop across the venturi and the collection efficiency for a gas cleaning application (Azzopardi et al., 1991). The purpose of this paper is to report an extension of the original

Correspondence concerning this article should be addressed to B. J. Azzopardi.

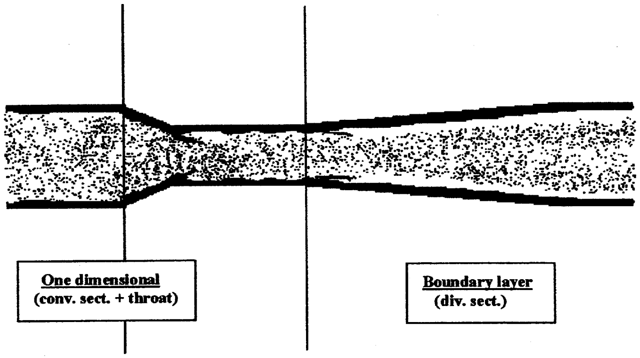

Figure 1. Venturi geometry and models used.

model, so that it can also be used for the measurement of a gas–liquid annular/dispersed flow just mentioned.

The new version of the model is presented in this article. The predictions of a computer code incorporating the model are compared with experimental data obtained at high pressure with hydrocarbon fluids. Pressure drop to the venturi throat, overall pressure loss, and pressure profiles are considered. It will be shown that a good agreement exists between predictions made with the modified model and experimental data.

Model for Annular/Dispersed Flow in a Venturi

The mathematical model that is used to describe the annular/dispersed flow through a venturi consists of a one-dimensional model for the convergent section and throat section of the venturi, and a quasi-one-dimensional (1-D) model incorporating an integral boundary-layer description for the divergent section (Figure 1). The requirement for the more complex approach in the diffuser arises from the difference in the sign of the pressure gradient that is present in these sections. In the convergent section and throat there is a favorable pressure gradient where pressure decreases with flow direction, the boundary layer becomes very thin, and the flow can be assumed to have a uniform velocity distribution about the cross section. In contrast, in the divergent section there is an unfavorable pressure gradient where the pressure increases with flow direction. From the start of the divergent section the flow is assumed to develop to a nonuniform profile with a significant growth of the boundary layer at the wall, which has been neglected in the 1-D model. A liquid film at the wall of the venturi is assumed to be present in the convergent section, the throat, and the divergent section.

1-D model for the convergent section and the throat

A 1-D annular/dispersed model describes the gas–liquid flow in the first two sections (convergent section and throat). As mentioned, a liquid film is assumed to be present at the wall. A dispersed phase of gas with droplets is present in the core region, so the presence of a very thin boundary layer at the gas–liquid interface is neglected. We will describe the flow quantitatively by a system of equations representing the mass and momentum balances. With these equations we can solve the unknown variables (gas and droplet velocities, pressure) as a function of the axial coordinate of the venturi.

Assuming we have n groups of droplets, the flow can be described by a system of $2n+2$ equations; a mass conservation equation for the gas, n mass conservation equations for the droplets, n momentum conservation equations for the droplets, and the pressure drop equation. With these equations we can solve $2n+2$ variables: the core velocity of the gas, the mass flow rates and the velocities of the n different droplet groups, and the pressure.

The mass conservation equation for the continuous gas phase is used in order to determine the gas velocity in the core at each axial position along the venturi
where

$$W_G = U_\infty \rho_G A$$

$$\frac{dW_G}{dx} = 0 \tag{1}$$

The velocity of the different groups of droplets (with different sizes) is determined by the drag force exerted by the gas on the droplets due to the velocity difference between gas and droplets. The following equations of motion are used to determine the velocities of the droplets in the different size groups

$$U_{D_i}\frac{dU_{D_i}}{dx} = \frac{3}{4}C_{D_i}\left(\frac{\rho_G}{\rho_L}\right)\frac{|U_\infty - U_{D_i}|\left(U_\infty - U_{D_i}\right)}{d_{D_i}} \tag{2}$$

where d_{D_i} is the mean droplet diameter of group i, calculated with the empirical correlation recommended by Azzopardi and Govan (1984)

$$d_{D_i} = \lambda_T\left(\frac{15.4}{We'^{0.58}} + \frac{3.5\rho_G W_{LE}}{\rho_L W_G}\right) \tag{3}$$

where $\lambda_T = \sqrt{\sigma/(\rho_L g)}$ is the Taylor wavelength and $We' = (\rho_L U_\infty^2 \lambda_T)/\sigma$ is the Weber number. This droplet-size equation accounts for the break up from the film (first term) and for coalescence (second term) (which particularly occurs at high liquid concentrations).

The drag coefficient is calculated with

$$C_{D_i} = \begin{cases} \dfrac{24}{Re_{D_i}}\left(1+0.15\,\mathrm{Re}_{D_i}\right)^{0.687} & \text{for } Re_{D_i} < 1{,}000 \\ 0.44 & \text{for } Re_{D_i} \geq 1{,}000 \end{cases} \tag{4}$$

where

$$Re_{D_i} = \frac{\rho_G |U_\infty - U_{D_i}| d_{D_i}}{\mu_G} \tag{5}$$

is the droplets' Reynolds number.

To determine the distribution of liquid between film and droplets we use mass-transfer equations in order to calculate the entrainment rate, E, and deposition rate, D, per unit area of channel wall at each axial position along the venturi

$$E = k_D C_E$$

$$D = k_D C \tag{5}$$

in which k_D is the mass-transfer coefficient (dependent on the surface tension) calculated from the correlation of Whalley et al. (1974), and C_E is the equilibrium concentration of entrained droplets, calculated from the correlation of Whalley and Hewitt (1978).

In these diffusion equations, C is the actual mass concentration of droplets given by

$$C = \sum_{i=1}^{n} \frac{W_{LE_i}}{AU_{D_i}} \tag{6}$$

Changes in mass flow rates of the liquid film and of the droplet groups (existing groups and the newly formed group) result from the entrainment and deposition rates at each position. The change in mass-flow rate of the liquid film is given by

$$\frac{dW_{LF}}{dx} = \pi d(D - E) \tag{7}$$

The mass-flow rate of newly formed droplets is determined by

$$\frac{dW_{LE_i}}{dx} = \pi dE \tag{8}$$

The Azzopardi−Govan relation determines the droplet diameter of the newly formed droplets. The change in mass-flow rates of the existing droplet groups is given by

$$\frac{dW_{LE_i}}{dx} = -\pi dD \frac{W_{LE_i}}{W_{LE}} \tag{9}$$

It has been observed that, in addition to the normal entrainment described by the preceding equations, there is additional entrainment that occurs at the boundary of the convergent and throat sections (Azzopardi and Govan, 1984; Fernandez Alonso et al., 1999). A smaller effect has been found at the throat diffuser boundary (Leith et al., 1984). Fernandez Alonso et al. gathered data from experiments with different convergence angles and provided correlations for the limiting condition for this extra entrainment, and for its magnitude their correlations had constants specific to each convergence angle. This information has been analyzed further and a single correlation developed. This has the form

$$\Delta E_f = 1 - 1.063\left(\frac{We_c}{We}\right)^{0.34} \tag{10}$$

where the critical Weber number for inception of extra entrainment is given by

$$We_c = 0.1857(90 - \theta/2) - 5.17 \tag{11}$$

with θ being the angle of convergence. Obviously, $\Delta E_f = 0$ for $We < 1.1968 We_c$. So it is assumed that the change in mass flow rate of an existing droplet group due to deposition is proportional to the mass-flow rate of that particular group relative to the total mass-flow rate of entrained liquid. The frictional effect of the flow is modeled through the shear stress at the interface between the gas-droplet core and the liquid film, and this stress is calculated through

$$\tau_i = \frac{1}{2} f_i(\rho_G + C_h) U_{GC}^2 \tag{12}$$

Here, the interfacial friction factor is given by $f_i = f_{GC}(1 + 360(m/d))$, as suggested by Wallis (1970). The gas and drops in the core are assumed to be traveling at the same velocity. The velocity of the mixture is given by

$$U_{GC} = \frac{W_G}{A\rho_G} + \frac{W_{LE}}{A\rho_L} \tag{13}$$

where W_G and W_{LE} are the mass-flow rates of gas and entrained liquid, respectively, and the contribution due to the droplets C_h is given by

$$C_h = \frac{W_{LE}}{AU_{GC}} \tag{14}$$

The smooth wall friction factor f_{GC} is calculated by

$$f_{GC} = \frac{0.079}{Re_{GC}^{0.25}} \tag{15}$$

where the Reynolds number for the homogeneous core is

$$Re_{GC} = \frac{(W_G + W_{LE})d}{A\mu_G} \tag{16}$$

The thickness of the liquid film, m, on the wall is derived by assuming that the ratio of the frictional pressure drop due to the film and the total frictional pressure drop is equal to the ratio of the liquid film cross-sectional area and the total cross-sectional area. The film thickness, m, is then calculated simultaneously with the interfacial shear stress using the relationship between film-flow-rate film thickness and frictional pressure drop

$$m = \sqrt{\frac{\left(\frac{d}{4}\right)^3 \left(\frac{dp}{dx}\right)_{LF}}{\tau_i}} \tag{17}$$

where Eq. 18 is the frictional pressure gradient that would be required if the liquid filled the cross section and flowed at the same average velocity

$$\left(\frac{dp}{dx}\right)_{LF} = \frac{2}{d} f_{LF} \rho_L U_{LF}^2 \tag{18}$$

This is the frictional pressure gradient that would occur when the liquid in the film occupied the total cross-section of the venturi and flowed with cross-sectional averaged velocity. The liquid-film friction factor is dependent on the liquid film Reynolds number

$$f_{LF} = \begin{cases} \dfrac{16}{Re_{LF}} & \text{for } Re_{LF} < 200 \\ \dfrac{0.079}{Re_{LF}^{0.25}} & \text{for } Re_{LF} > 8{,}000 \\ \dfrac{143.38}{(\ln Re_{LF})^{4.5}} + 0.001069 & \text{for } 200 \leq Re_{LF} \geq 8{,}000 \end{cases} \tag{19}$$

and the liquid-film Reynolds number is given by $\mathrm{Re}_{LF} = (G_{LF} d/\mu_L)$, where $G_{LF} = W_{LF}/A$ is the mass flux of the liquid film.

The momentum equation for the gas-droplet core is solved in order to calculate the pressure at the various positions along the venturi. According to this equation, the acceleration of the gas, the acceleration or deceleration term for the droplet groups (dependent on the relative velocity of the particular droplet group), and the friction at the interface between the core and the liquid film determine the pressure gradient. The pressure derivative is integrated with a fourth-order Runge−Kutta subroutine

$$-\frac{dp}{dx} = \frac{W_G}{A}\frac{dU_\infty}{dx} + \sum_{i=1}^{n} \frac{W_{LE_i}}{A}\frac{dU_{D_i}}{dx} + \frac{4\tau_i}{d} \tag{20}$$

Boundary-layer model for the divergent section

In the divergent section of the venturi a boundary-layer model is used to describe the flow, because of the unfavorable adverse pressure gradient that is present here. The flow in this section is divided in two regions: the core region and the boundary-layer region. In the core region the flow of gas and droplets is described as in the one-dimensional model. In the boundary-layer region it is assumed that there are no droplets, and the flow is modeled as a viscous flow over a rough surface. In the boundary-layer model we make use of a group of characteristic variables. These parameters are directly or indirectly dependent on the boundary-layer thickness, δ, and are defined as:

The blockage parameter: $B = \delta^*/R$;
The blockage fraction: $\Lambda = \delta^*/\delta$,
The boundary-layer shape factor: $H = \delta^*/\theta$,
The shape factor: $h = (H-1)/H$.

In fact, by defining these parameters, we use two independent variables in the modeling: the displacement thickness, δ^*, and the momentum thickness θ.

Boundary-layer region

The boundary-layer region is quantitatively described by a system of equations consisting of a two-phase momentum integral equation (together with an assumed wall-wake velocity profile) and a boundary-layer entrainment equation (together with a correlation for the boundary layer entrainment rate).

A momentum balance over the boundary-layer region (in which the pressure at the edge of the boundary layer is taken into account) results in the following momentum integral equation

$$\frac{d\theta}{dx} + (2+H)\frac{\theta}{U_\infty}\frac{dU_\infty}{dx} + \frac{\theta}{R}\frac{dR}{dx} + \delta\left(\frac{\rho_L}{\rho_G}\right)\frac{1}{U_\infty^2}\sum_{i=1}^{n} \phi D_i U_{D_i}\frac{dU_{D_i}}{dx} = \frac{C_f}{2} \tag{21}$$

in which ϕ_{D_i} is the volume fraction of each group of drops, $C_f = k^2 V_T |V_T|$ is the skin friction coefficient, and k is the Von Karman constant (= 0.41). The nondimensional shear velocity V_T ($= u_\tau(kU_\infty)$ is obtained from integrating the fully rough form of the Coles wall-wake velocity profile over the boundary layer. This results in

$$V_T = \frac{1-2\Lambda}{\ln \dfrac{Re^*}{\Lambda} - \ln Re_\epsilon + 1.485} \tag{22}$$

The Reynolds number based on the displacement thickness δ^* is defined as $Re^* = U_\infty \delta^*/\nu$, and the Reynolds number based on the liquid film roughness is given by $Re_s = U_\infty \epsilon/\nu$. The roughness height is dependent on the thickness of the liquid film and is given by

$$\epsilon = Km \tag{23}$$

The original value of K had been taken from publications on annular flow in vertical pipes. There, for wide ranges of flow rates, the interface is dominated by large, fast-moving structures usually called disturbance waves. These have been seen in venturis at higher film flow rates. The height of these disturbance waves was five times the mean film thickness. A value of $K = 5$ was considered reasonable. In contrast, in both pipe flows and venturis, when the film flow rates are low, there are no disturbance waves and the interface is covered by ripples of much lower amplitude and celerity. A much lower value of K is needed. In the present work a value of 0.085 was chosen.

A mass balance over the boundary-layer region gives us the boundary-layer entrainment equation

$$\frac{1}{RU_\infty}\frac{d}{dx}\left[RU_\infty(\delta - \delta^*)\right] = E_b \tag{24}$$

where E_b is the dimensionless boundary-layer entrainment rate, which is determined from the correlation suggested by Ferziger et al. (1982), that is

$$E_b = 0.0083(1-\Lambda)^{-2.5} \tag{25}$$

Core region

In the core region we have the continuity equation, $dQ/dx = 0$, where the cross section of flow is reduced due to the presence of the boundary layer. The volumetric flow rate, in which the volume fraction of the droplets has been neglected, is given by

$$Q = U_\infty \pi R^2 (1 - B)^2 = U_\infty \pi (R - \delta^*)^2 \quad (26)$$

Using this flow-rate equation, the mass-continuity equation can be written as

$$\frac{1}{U_\infty}\frac{dU_\infty}{dx} = \frac{2}{1-B}\frac{dB}{dx} - \frac{2}{R}\frac{dR}{dx} \quad (27)$$

The pressure is calculated as in the convergent section and throat (again taking the deposition, entrainment, and acceleration or deceleration of the droplets into account).

Calculation procedure

The model consists of a number of ordinary differential equations. For the convergence and throat sections, they consist of drop and film mass balances, Eqs. 7 and 8 using Eq. 5 to specify the fluxes of entrainment and deposition; drop acceleration, Eq. 2 using Eq. 4 to specify drag coefficient and Eq. 3 for drop size; pressure drop, Eq. 1. The possibility of drops being created all along the venturi is allowed for by tracking separate groups of drops. In the diffuser section additional equations are provided for the blockage parameter, B, and the boundary-layer blockage fraction, Λ, from a combination of Eqs. 21 to 27. The initial values of drop velocities are taken to be 10% of the local gas velocity. Initial values of the division of liquid between film and drops and of B and Λ are specified. The equations have been incorporated into a Fortran computer program and integrated along the venturi from initial values using a fourth-order Runge–Kutta–Merson numerical procedure. For this particular application it is important to know how much liquid is traveling as drops at the entrance of the venturi and the size of those drops. The methods used for these parameters are discussed below.

Experimental Data

Two sets of experimental data have been used to test the model described in the second section. The first was obtained at the wet-gas test facility of CEESI in Colorado, USA. The venturi was installed in a 0.097-m-diam. pipe and had a 0.058-m-diam. throat one diameter long. The convergence and diffuser angles were 30° and 7°, respectively. The fluids employed were methane and decane. The ranges of pressures, gas upstream velocities, and liquid loading are given in Table 1.

The fraction of liquid in the flow (the so-called wetness of the gas) is often expressed by the Lockhart–Martinelli parameter X. For the CEESI data-set, X ranges from 0 to 0.15.

Table 1. Ranges of Parameters Used in Experiments

P (bar)	U_G (m/s)	Liquid Loading (W_L/W_G) (%)
14	3–12	0–50
48	3–12	0–50
83	3–12	0–50

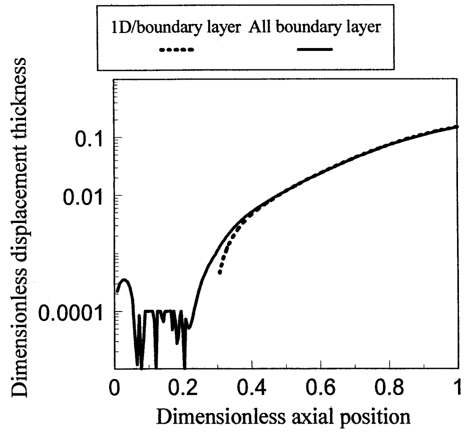

Figure 2. Axial distribution of dimensionless displacement thickness showing agreement between the 1-D/boundary-layer model and the all-boundary-layer model.

The second set of data was obtained at the SINTEF facility in Norway. Here the venturi was installed in a 0.097-m-diam. pipe and had a 0.039-m-diam. throat approximately one diameter long. The convergence and diffuser angles were 21.5° and 7.65°, respectively. Pressures in the range 15–90 bar, gas upstream velocities of 7–12 m/s, and liquid loadings up to 81% by mass were used. The fluids employed were nitrogen and diesel.

Sensitivity of the Model

Before testing the model against the experimental data described in the third section, tests were carried out to establish the sensitivity of the model. A first test considered the simplification of ignoring the boundary layer in the convergence and throat sections on the grounds that it would be thin enough to be negligible. This was tested using a second com-

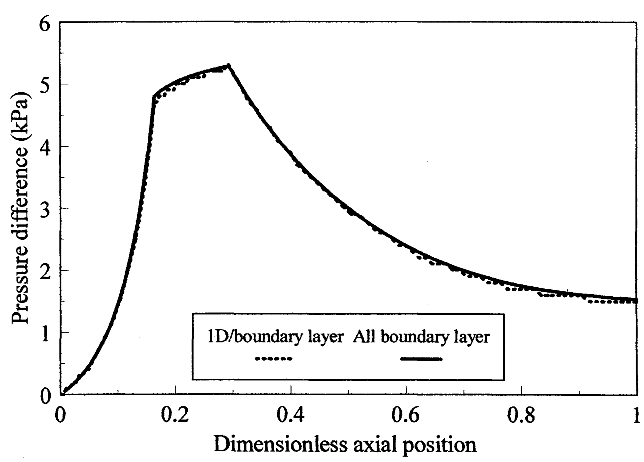

Figure 3. Axial pressure profiles showing agreement between 1-D/boundary-layer model and the all-boundary-layer-model.

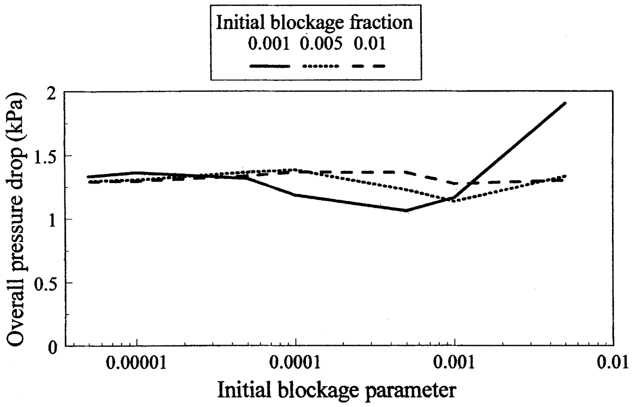

Figure 4. Effect of initial boundary-layer parameters on overall pressure drop.

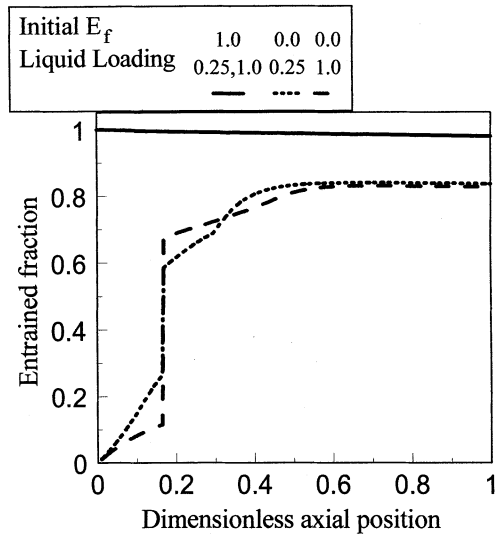

Figure 5. Axial variation of entrained fraction showing effect of initial entrained fraction and of liquid loading.

puter program that used the boundary-layer model all along the venturi. Figure 2 shows the predicted boundary-layer thickness, as dimensionless momentum thickness, for both cases. As can be seen, the boundary layer is indeed negligibly thin, and both models give equivalent boundary-layer growth in the diffuser. Figure 3, which presents the pressure difference along the venturi, again shows no difference between the two predictions.

The effect of the values of the initial conditions of the boundary-layer parameters, B_o and Λ_o, were considered in the second test of sensitivity. Figure 4 shows the result of one such test and illustrates the lack of sensitivity to these parameters.

The third test concerns the initial distribution of liquid between film and drops. Here calculations have been carried out for two extreme cases, entrained fraction = 0 and = 1. Runs were carried out at a typical liquid loading (25% liquid to gas by mass) and for one greater than the usual scope of wet-gas meters (100% liquid to gas by mass). Figure 5 shows the variation of the entrained fraction along the venturi, while Figure 6 illustrates the pressure-difference profiles. The results indicate that, for the all-drops cases, little deposition occurs. When the liquid is introduced as a film, there is a continuous increase in entrained fraction with a very noticeable step change at the start of the throat. The effect of the initial entrained fraction is also clearly visible in the pressure-difference profile. Pressure differences are higher for all the flow entering as a film, because the newly created drops have to be accelerated over a greater difference in velocity. These results should be considered in the context of entrained fractions expected in gas production fields. Although there is considerable literature on entrained fraction in vertical upward flow, data for horizontal pipes are more limited. Moreover, these studies tend to be confined to air/water flows. An exception to this is found in the work of Hoogerndoorn and Welling (1965), who used pipes up to 0.1 m in diameter and employed low surface-tension liquids. The correlation they propose suggests that entrained fractions will be 1.0.

The effect of the initial drop size has also been considered. The equation suggested by Azzopardi and Govan (1984) (Eq. 3), was originally derived from data from upward annular flow in vertical pipes. The data were obtained from pipes 0.01–0.127 m in diameter. The fluids were mainly air/water, though both surface tension and gas density were tested in the smallest-diameter pipe. Recent data from air/water experiments in a 0.095-m-dia. horizontal pipe (Simmons and Hanratty, 2001) have permitted a further test of Eq. 3. Here the predictions were within 0% to −33% of the measured values. To cover a slightly greater range, calculations were carried out with drop sizes equal to and ±50% of the values given by Eq. 3. The results are presented in Figure 7, where an effect of drop size can be seen. However, the effect is not as great as the drop-size variation with errors of +13.3% to

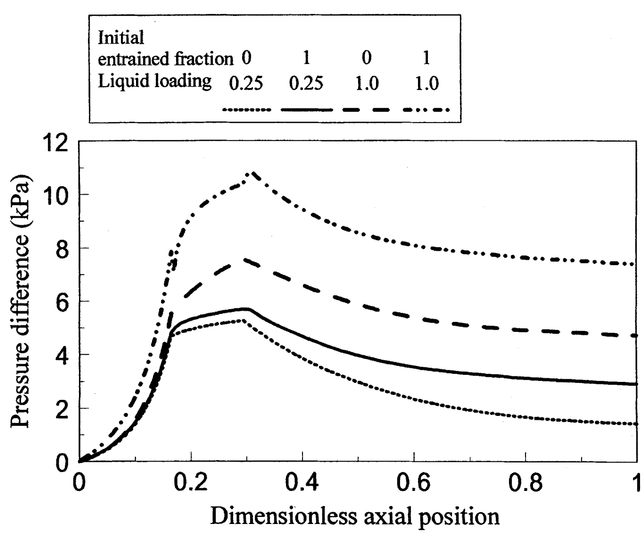

Figure 6. Axial variation of pressure-difference showing effect of initial entrained fraction and of liquid loading.

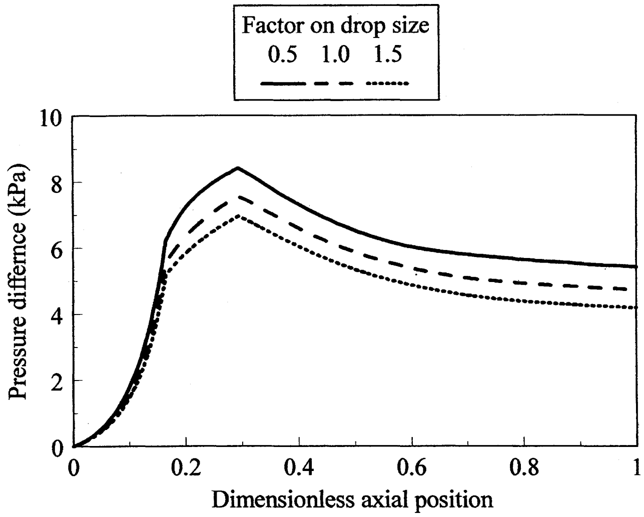

Figure 7. Effect of initial drop size on pressure difference profile.

−8.1% for the pressure drop to the throat and +14.6% to −11.5% for the total pressure drop across the venturi.

Comparisons Between Model Predictions and Experimental Data

Comparisons were made between the experimental data and predictions made with the theoretical model described in the preceding section. The data used for the comparison were chosen in such a way that they cover the full ranges of parameters varied in the experiments. Initial comparisons were made for single-phase flow. Figure 8 shows good agreement with experimental data for both pressure drop to the venturi throat and overall pressure drop. Also shown is the value of

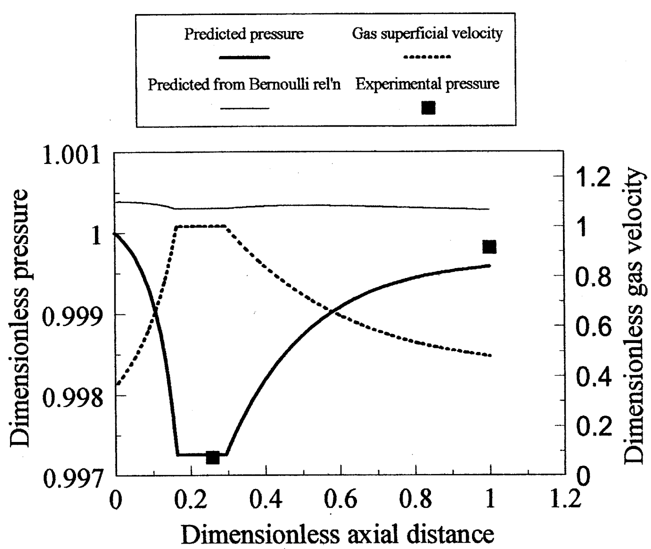

Figure 8. Pressure profile, velocity variation, and Bernoulli's constant for single-phase flow without viscosity.

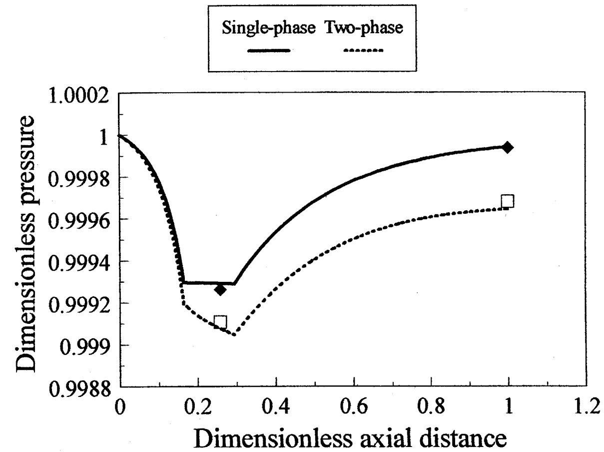

Figure 9. Predictions of pressure profiles compared to experimental data.

the mechanical energy that characterized Bernoulli's law. Only a small variation in the mechanical energy is seen (about 4%). This is due to the variation of the density along the venturi.

From the sensitivity results shown in Figure 4, inlet values of the boundary-layer parameters B and Λ were set to 10^{-4} 10^{-3}, respectively. The model is shown to predict both single-phase and two-phase data successfully (Figure 9). Similar agreement was found over the ranges of pressures, gas flow rates, and liquid loading that were used in the experiments.

Attention was given to the possibility of separation (or sometimes called detachment) of the boundary layer. Although the theoretical model is capable of dealing with separation of the boundary layer in the divergent section, numerical problems arise when separation really occurs. However, no separation of the boundary layer is obtained for the conditions in this work.

The split of liquid between film and drops can be expressed through the entrained fraction. Figure 10 shows a comparison between total pressure drops measured at CEESI and predictions made with the modified model as a function of the liquid load for two initial values of the entrained liquid fraction at the start of the venturi. Values are shown for all liquid initially traveling as film or all as drops. It can be seen that the total pressure drops show an almost linear relationship with the liquid load (for high values of the liquid loads). The pressure drop is higher for the initially low entrainment case because here the film flow rate is higher, above the critical value for the occurrence of disturbance waves, and, thence, the roughness/film thickness ratio takes the higher value.

Figures 11 and 12 reveal that predictions of the pressure drop (made with the modified model) are in good agreement with experiments when the experiments were in annular/dispersed flow. Predictions made for experiments from stratified-wavy flow were poorer. This can be expected, as the model is based on the assumption of annular/dispersed flow. The determination of the flow regime is based on the method taken from Oliemans (1998).

The model also gave good predictions of the experimental results obtained at the SINTEF facility. Figures 13 and 14

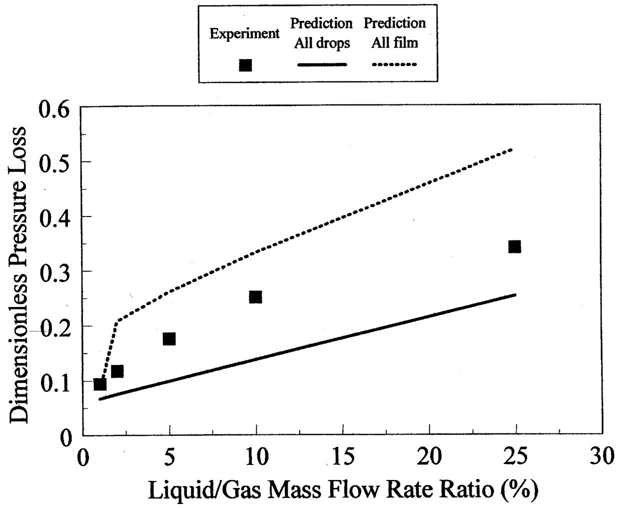

Figure 10. Recovery differential pressures against liquid loading for the extreme inlet values of the entrained fraction.

show comparisons, at 30 and 90 bar. Again good agreement is obtained and shows that the effect of a different geometry and a different fluids pair, nitrogen–diesel oil instead of methane–decane, can be handled. The SINTEF data set covers four different line pressures. Good agreement was obtained over the ranges of pressures.

Conclusions

(1) For annular/dispersed flow, the modified model is in good agreement with the CEESI data and the SINTEF data.

(2) The range of applicability of the model seems promising, since application of the modified model to completely different experiments (different venturi geometry and different fluid pairs in the SINTEF experiments compared to the CEESI experiments) gives good predictions for all cases.

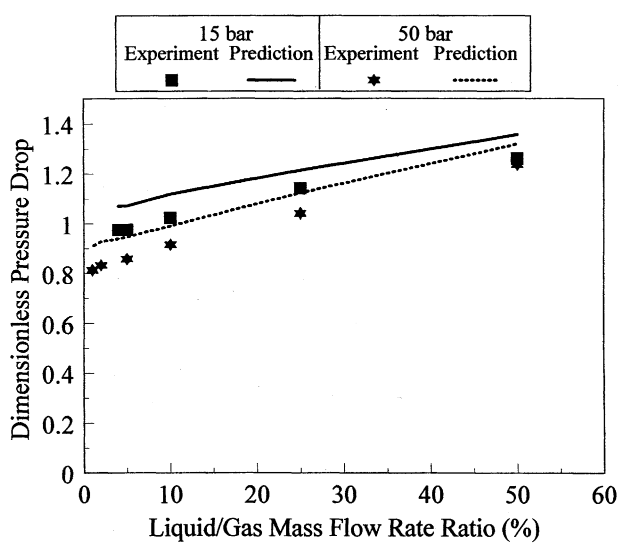

Figure 11. Venturi differential pressures as a function of liquid loading for stratified-wavy flow.

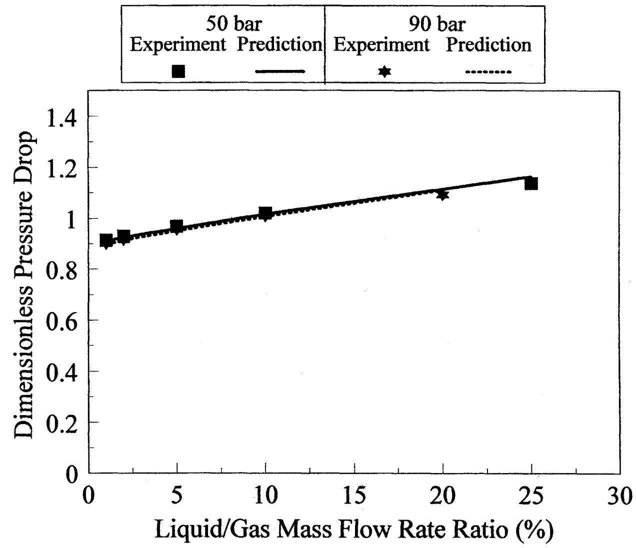

Figure 12. Venturi differential pressures against liquid loading for annular-dispersed flow.

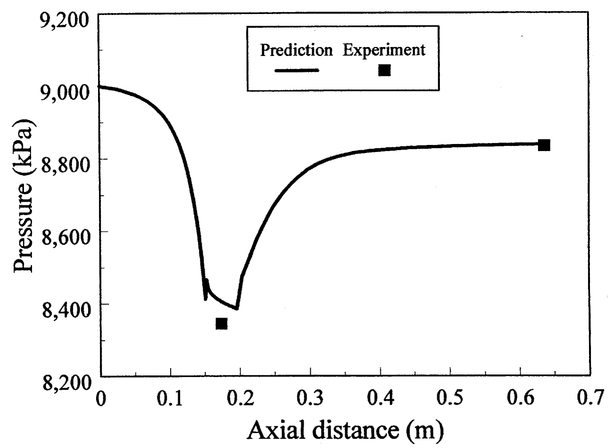

Figure 13. Pressure prediction with the modified model compared to SINTEF data, 90 bar.

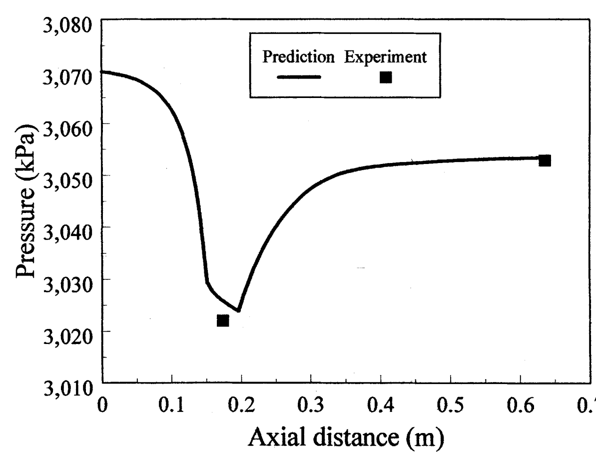

Figure 14. Pressure prediction with the modified model compared to SINTEF data, 30 bar.

(3) Further work is required to determine how the model can be adapted to the stratified-wavy flow pattern.

Notation

A = cross-section surface area, m^2
B = boundary-layer parameter
C = droplet concentration, kg/m^3
C_D = drag coefficient
C_E = equilibrium concentration, kg/m^3
C_f = skin friction factor
C_h = homogeneous droplet concentration, kg/m^3
d = local diameter, m
d_D = droplet diameter, m
D = deposition rate, $kg/m^2 \cdot s$
E = entrainment rate, $kg/m^2 \cdot s$
E_b = boundary-layer entrainment rate
E_f = entrained fraction
f = fanning friction factor
g = gravitational acceleration, m/s^2
G = mass flux, $kg/m^2 \cdot s$
h = shape factor
H = boundary-layer shape factor
k = Von Karman constant (= 0.41)
k_D = mass-transfer coefficient, m/s
K = roughness/film-thickness ratio
M = thickness of liquid film, m
N = total number of droplet groups
P = local pressure, $kg/m \cdot s^2$
dp/dx = local pressure derivative, $kg/m^2 \cdot s^2$
$(dp/dx)_{LF}$ = frictional pressure gradient due to the liquid film, $kg/m^2 \cdot s^2$
Q = volume flow rate, m^3/s
R = local radius, m
Re = Reynolds number
Re_D = droplet Reynolds number
Re_{GC} = homogeneous-core Reynolds number
Re_{LF} = liquid-film Reynolds number
Re_ϵ = Reynolds number based on liquid-film roughness
Re^* = Reynolds number based on displacement thickness
U = local velocity, m/s
U_G = gas velocity approaching the venturi, m/s
U_∞ = core velocity, m/s
V_T = nondimensional shear velocity
W = mass flow rate, kg/s
We' = Weber number
x = axial distance, m
X = Lockhart−Martinelli parameter

Greek letters

δ = boundary-layer thickness, m
δ^* = displacement thickness, m
ϵ = liquid-film mean roughness height, m
ϕ_{Di} = volume fraction of each group of drops
λ_T = Taylor wavelength, m
Λ = boundary-layer blockage fraction
μ = viscosity, $kg/m \cdot s$
ν = kinematic viscosity, m^2/s
θ = momentum thickness, m
ρ = density, kg/m
σ = surface tension, kg/s
τ_i = interfacial shear stress, $kg/m \cdot s^2$

Subscripts

D = droplet
G = gas
GC = homogeneous annular flow core
i = group of droplets
L = liquid
LE = entrained liquid in the core region
LF = liquid film at the venturi wall
o = initial value
∞ = core

Literature Cited

Azzopardi, B. J., and A. H. Govan, "The Modelling of Venturi Scrubbers," *Filtr. Sep.*, **21**, 196 (1984).

Azzopardi, B. J., S. F. C. F. Teixeira, A. H. Govan, and T. R. Bott, "An Improved Model for Pressure Drop in Venturi Scrubbers," *Trans. Inst. Chem. Eng.*, **69B**, 237 (1991).

Brook, N., "Flow Measurement of Solid-Liquid Mixtures Using Venturi and other Meters," *Proc. Inst. Mech. Eng.*, **176**, 127 (1962).

Fernandez Alonso, D., B. J. Azzopardi, and J. H. Hills, "Gas/Liquid Flow in Laboratory-Scale Venturis," *Trans. Inst. Chem. Eng.*, **77B**, 205 (1999).

Ferziger, J. H., A. A. Lyrio, and J. G. Bardina, "New Skin Friction and Entrainment Correlations for Turbulent Boundary Layers," *Trans. ASME, J. Fluids Eng.*, **104**, 537 (1982).

Graf, W. H., "A Modified Venturimeter for Measuring Two-Phase Flow," *J. Hydraul. Res.*, **5**, 161 (1967).

Hall, A. R. W., M. J. Reader-Harris, and B. C. Millington, "A Study of the Performance of Venturi Meters in Multiphase Flow," North American Conf. on Multiphase Technology, Banff, Alta., Canada, (2000).

Harris, D. M., "Calibration of a Steam Quality Meter for Channel Power Measurement in the Prototype," S. G. H. W Reactor. European Two-Phase Flow Group Meeting, Bournmouth, UK (1967).

Hirata, Y., M. Takano, and T. Narasaka, "Measurements of Flow Rates and Particle Concentrations in Heterogeneous Solid-Water Two-Phase Flows by Means of a Venturi," *JSME Int. J.*, **34B**, 304 (1991).

Hirata, Y., M. Takano, and T. Narasaka, "Simultaneous Measurements of Flow Rates and Particle Concentrations in Heterogeneous Solid-Water Two-Phase Flows by Means of One Venturi," *JSME Int. J.*, **38B**, 440 (1995).

Hoogerndoorn, C. J., and W. A. Welling, "Experimental Studies on the Characteristics of Annular Mist Flow in Horizontal Pipes." Symposium on Two Phase Flow, Exeter, UK (1965).

Leith, D., K. P. Martin, and D. W. Cooper, "Liquid Utilisation in a Venturi Scrubber," *Filtr. Sep.*, **21**, 191 (1984).

Machado, R. T. M., "Multiphase Flow in a Venturi: an Experimental and Theoretical Study," PhD Thesis, Imperial College, London (1997).

Oliemans, R. V. A., "Applied Multiphase Flow," Lecture notes. Dept. of Applied Physics, Delft Univ. of Technology, Delft, The Netherlands (1998).

Pinheiro da Silva Filho, J. A., DIC Thesis, Imperial College, London (2000).

Simmons, M. J. H., and T. J. Hanratty, "Droplet Size Measurements in Horizontal Annular Gas-Liquid Flow," *Int. J. Multiphase Flow*, **27**, 861 (2001).

Thompson, J. G., H. Hacking, and M. G. Cuthbertson, "S.G.H.W.R. Steam Meter Calibration Trails," BSRA Marine Engineering Contract Report No. W.46 (1966).

Wallis, G. B., "Annular Two-Phase Flow: Part 2 Additional Effects," *J. Basic Eng.*, **92**, 73 (1970).

Whalley, P. B., P. Hutchinson, and G. F. Hewitt, "The Calculation of Critical Heat Flux in Forced Convection Boiling," *Heat Transfer 1974*, Vol. 4, Scripta Book Co., p. 290 (1974).

Whalley, P. B., and G. F. Hewitt, "The Correlation of Liquid Entrainment Rate in Annular Two-Phase Flow," UKAEA Report AERE R-9187 (1978).

Manuscript received Mar. 29, 2002, and revision received Nov. 13, 2002.